Molecular dynamics study of $CaSiO_3$–$MgSiO_3$ glasses under high pressure

2006 J. Phys.: Condens. Matter 18 6531

(http://iopscience.iop.org/0953-8984/18/28/008)

INSTITUTE OF PHYSICS PUBLISHING JOURNAL OF PHYSICS: CONDENSED MATTER

J. Phys.: Condens. Matter **18** (2006) 6531–6544 doi:10.1088/0953-8984/18/28/008

Molecular dynamics study of $CaSiO_3$–$MgSiO_3$ glasses under high pressure

Keiji Shimoda[1,2] **and Masayuki Okuno**[1]

[1] Department of Earth Sciences, Faculty of Science, Kanazawa University, Kanazawa 920-1192, Japan
[2] Advanced Technology Research Laboratories, Nippon Steel Corporation, 20-1 Shintomi Futtsu, 293-8511, Japan

E-mail: kshimoda@re.nsc.co.jp

Received 1 May 2006, in final form 22 May 2006
Published 28 June 2006
Online at stacks.iop.org/JPhysCM/18/6531

Abstract

The pressure-induced structural evolutions of $CaSiO_3$–$MgSiO_3$ glasses have been examined by means of molecular dynamics simulation. Our calculations revealed that Si coordination remained unchanged up to 15 GPa, while modifier cations caused significant changes in the short-range order structure. In the present study, we conclude that the main compression mechanisms for $CaSiO_3$–$MgSiO_3$ glasses are: (1) the Si–O–Si angle reduction, (2) the coordination increase of Ca and Mg cations, and (3) the compaction in the medium-range scale. Furthermore, small changes in the Q^n distribution suggest pressure-induced disproportionation reactions. Similar pressure responses between $CaSiO_3$–$MgSiO_3$ glasses may imply that the structural changes of SiO_4 framework units are more significant than those of interstitial cations, Ca and Mg.

1. Introduction

Structural information on silicate melts and glasses under pressure is of geological interest for understanding physical and thermodynamic behaviours of magmatic liquids under the Earth's crust and mantle. Several experimental techniques such as x-ray and neutron diffraction, x-ray absorption spectroscopy (XAS), Raman and infrared (IR) spectroscopy and nuclear magnetic resonance (NMR) spectroscopy have been applied for the purposes. Also, theoretical approaches, such as molecular dynamics (MD) simulation, can provide detailed information on the properties that are experimentally inaccessible.

Intensive studies have been carried out on SiO_2 glass/melt under pressure, because of its importance for geological and industrial applications (Tse *et al* 1992, Jin *et al* 1993, 1994, Tsuneyuki and Matsui 1995, Valle and Venuti 1996, Ekunwe and Lacks 2002, Trachenko and Dove 2003, Pilla *et al* 2003). On the other hand, there have only been a few MD studies on

Table 1a. Empirical potential parameters used in this study (Miyake 1998).

Ion	z (e)	a (Å)	b (Å)	c (kJ$^{1/2}$ Å^3 mol$^{-1/2}$)	Ion pair	D (kJ mol^{-1})	β (Å^{-1})	r^* (Å)
Ca	0.96	1.1425	0.042	30.74	Ca–O	21.0	2.0	2.20
Mg	0.96	0.9400	0.040	20.49	Mg–O	42.0	2.0	1.75
Si	1.92	0.5983	0.025	0.00	Si–O	63.0	2.0	1.47
O	−0.96	1.7700	0.138	51.23				

Table 1b. Experimental and MD-derived cell parameters for the $CaSiO_3$–$MgSiO_3$ system at 0.1 MPa and 300 K (Miyake 1998).

		a (Å)	b (Å)	c (Å)	α (deg)	β (deg)	γ (deg)
Wollastonite	Exp.[a]	7.940	7.320	7.070	90.033	95.367	103.433
($CaSiO_3$)	MD	7.700	7.335	7.102	90.080	93.216	103.861
Diopside	Exp.[b]	9.746	8.899	5.251	90	105.63	90
($CaMgSi_2O_6$)	MD	9.856	8.814	5.292	89.994	105.838	90.006
Enstatite	Exp.[c]	18.225	8.813	5.180	90	90	90
($MgSiO_3$)	MD	18.554	8.702	5.208	90.003	89.998	90.009
Clinoenstatite	Exp.[d]	9.626	8.825	5.188	90	108.33	90
($MgSiO_3$)	MD	9.746	8.695	5.200	89.997	107.813	90.007

[a] Peacor and Prewitt (1963).
[b] Clark *et al* (1969).
[c] Ohashi (1984).
[d] Morimoto (1960).

alkaline earth silicate glasses, in spite of the geological significance of these compositions. Kubicki and Lasaga (1991) have reported the structural evolutions of $MgSiO_3$ and Mg_2SiO_4 glasses/melts with increasing pressure by MD simulation with a set of parameters derived quantum-mechanically. Matsui (1996) compared the MD-derived molar volumes, bulk moduli and thermal expansivities for $CaSiO_3$–$MgSiO_3$ melts at 1900 K with the available experimental data. He also reported the coordination changes of Si, Ca and Mg cations with pressure. In the present study, we pursue the detailed structural modification on $CaSiO_3$–$MgSiO_3$ glasses up to 15 GPa, examining the compression mechanisms before the Si coordination change begins.

2. Methodology of MD simulation

We performed a set of MD simulations using MXDORTO codes developed by Kawamura (1996). In the present study, an interatomic potential function (Φ_{ij}) between atoms i and j consists of Coulombic, short-range repulsion, van der Waals attraction, and Morse potential terms as given by

$$\Phi_{ij}(r_{ij}) = \frac{z_i z_j e^2}{r_{ij}} + f_0(b_i + b_j)\exp\left(\frac{a_i + a_j - r_{ij}}{b_i + b_j}\right) - \frac{c_i c_j}{r_{ij}^6} + D_{ij}\left\{\exp\left[-2\beta_{ij}(r_{ij} - r_{ij}^*)\right] - 2\exp\left[-\beta_{ij}(r_{ij} - r_{ij}^*)\right]\right\}$$

where r_{ij} is the interatomic distance, f_0 (=6.9511×10^{-11} N) a constant, e the electronic charge, z, a, b and c parameters for each atomic species, and D_{ij}, β_{ij} and r_{ij}^* parameters for cation–anion pairs. The Morse term was applied to Si–O, Mg–O, Ca–O pairs. These parameters were derived empirically (Miyake 1998; table 1a) to simulate the structures of feldspar and pyroxene and some high-pressure minerals (table 1b). The parameters allowed the successful reproduction of the cell dimensions of clinoenstatite at room temperature and their changes with

temperature up to at least 2000 K at 0.1 MPa. (Shimobayashi *et al* 2001). The Ewald method was used for the summation of Coulombic interactions. Equations of motion of ions were solved numerically using the Verlet algorithm with a time increment of 2.0 fs (2.0×10^{-15} s). Temperature and pressure were controlled by scaling particle velocities and simulation cell parameters, respectively (*NPT* ensemble).

A periodic boundary condition was applied to the orthorhombic simulation cells containing 2000 atoms. The initial structure of each system was generated randomly and the system was equilibrated at 4000 K for 500 000 steps (1.0 ns). Then, the temperature was reduced to 3500 K at a rate of −0.01 K/step and equilibrated for another 950 000 steps (1.9 ns). This process was repeated down to 3000, 2500, 2000, 1500, 1000 K and finally the temperature was reduced to 300 K with another 950 000-step equilibration. After the equilibration at 0.1 MPa, homogeneous pressures were imposed up to 15 GPa with a 2.5 GPa step. At each pressure 1000 000-step equilibration was achieved for structural relaxation.

Pair correlation functions (PCFs) are commonly used to investigate short-range order in amorphous materials. This gives the probability density of finding an ion within an interval Δr at a distance r from a specified particle. The pair correlation function $g_{ij}(r)$ is defined as

$$g_{ij}(r) = \frac{V}{N^2}\left\langle \sum_{i=1}^{N} \sum_{\substack{j=1 \\ j\neq i}}^{N} \delta(r - r_{ij}) \right\rangle.$$

The PCFs are time-averaged over all configurations generated during the production run. The x-ray interference function, $S{\cdot}i(S)$, can be calculated using the MD-derived pair correlation function, $g_{ij}(r)$:

$$S{\cdot}i(S) = \sum_i \sum_j N_i N_j f_i(S) f_j(S) \Big/ \left[\sum_k N_k f_k(S)\right]^2 \times \int 4\pi\rho r \left[g_{ij}(r) - 1\right] \sin(Sr)\, \mathrm{d}r.$$

3. Results

Figure 1 shows MD-derived atomic configurations of $CaSiO_3$ and $MgSiO_3$ glasses. The amorphous structures differ from the crystalline counterparts, wollastonite and enstatite. Figure 2 represents the equations of state for MD-derived $CaSiO_3$–$MgSiO_3$ glasses at 300 K. This suggests that there is no significant difference in the compressibility between $CaSiO_3$–$MgSiO_3$ glasses.

Figures 3 and 4 show the pair correlation functions (PCFs) of $CaSiO_3$ and $MgSiO_3$ glasses at 0.1 MPa, 7.5 and 15 GPa at 300 K. At 0.1 MPa and 300 K, the MD-averaged Si–O distance and Si coordination number were 1.62 Å and 4.0, respectively. The Si–Si distance and Si–O–Si bond angle were 3.17 Å and 148.4°. Also, average Ca–O and Mg–O distances were at 2.34 and 2.07 Å, and the Ca and Mg coordination numbers were calculated to be 6.5 and 5.7, respectively.

At 15 GPa and 300 K, Si–O and Si–Si distances were at 1.60 and 3.06 Å. Average Si–O–Si bond angle was ∼138°. Ca–O and Mg–O distances were 2.28 and 2.04 Å, respectively. The Ca and Mg coordination numbers were calculated to be 7.9 and 6.6. We observed a decrease of interatomic distances, a narrowing of bond angle and an increase of cation coordination numbers with increasing pressure. These are listed in tables 2 and 3.

Figures 5(a) and 6(a) show MD-derived $S{\cdot}i(S)$ curves for $CaSiO_3$ and $MgSiO_3$ glasses at 0.1 MPa, with contributions decomposed into SiO_4-associated (O–O, Si–O and Si–Si), and Ca- or Mg-associated (Ca–O, Ca–Si and Ca–Ca for $CaSiO_3$ and Mg–O, Mg–Si and Mg–Mg for $MgSiO_3$) components. Figures 5(b) and 6(b) represent the $S{\cdot}i(S)$ curves for $CaSiO_3$ and

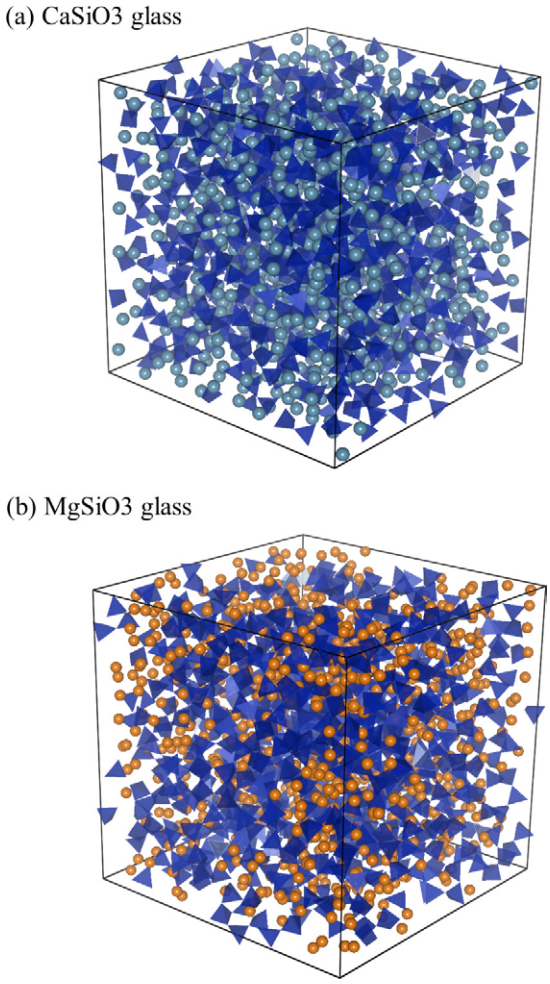

Figure 1. Atomic configurations of $CaSiO_3$ (a) and $MgSiO_3$ (b) glasses at 0.1 MPa and 300 K. The tetrahedra indicate SiO_4 units and the balls are modifier cations. They were drawn with the VENUS program developed by Dilanian, Izumi and Monma.

(This figure is in colour only in the electronic version)

$MgSiO_3$ glasses at 0.1 MPa, 7.5 and 15 GPa. There are significant changes in the low-S region with pressure, suggesting that significant modifications in medium-range order structure.

Information on network connectivity is an important aspect for determining macroscopic properties. The Q^n distribution of $CaSiO_3$–$MgSiO_3$ glasses is plotted in figure 7, as a function of pressure. Q^n indicates the polymerized species in the glass structure, and the subscript n denotes the number of bridging O atoms within a SiO_4 tetrahedron ($n = 0$–4). The Q^n distributions of $CaSiO_3$ and $CaMgSi_2O_6$ glasses show a Q^2-dominance in the structures at ambient pressure. On the other hand, $MgSiO_3$ glass is Q^3-dominant with a broad distribution of Q^1–Q^4 species. Although the pressure variations in Q^n species seem to be small (<5%), a slight increase of Q^3 species accompanying a decrease of Q^2 species is observed at high pressures.

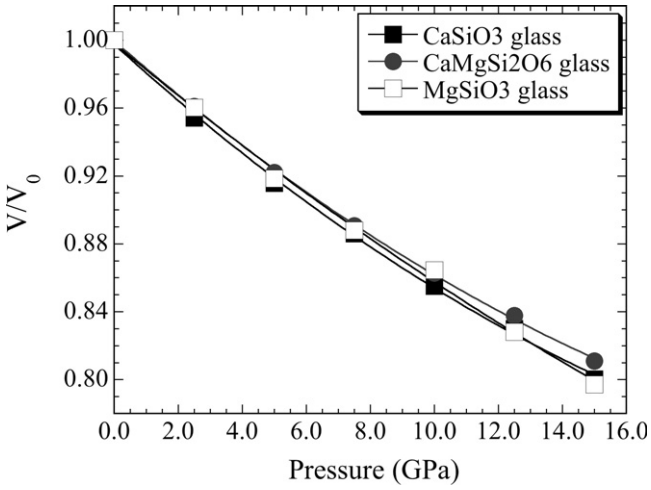

Figure 2. Equations of state for $CaSiO_3$–$MgSiO_3$ glasses at 300 K.

Table 2. A list of interatomic distances, bond angles and coordination numbers for $CaSiO_3$ glass at 300 K. The cut-off distances for Si–O and Ca–O coordination are 2.0 and 3.0 Å, respectively.

	Interatomic distance (Å)		Coordination number	Bond angle (deg)	
0.1 MPa	O–O	2.64	—	O–Si–O	109.3
	Si–O	1.62	4.0	Si–O–Si	148.6
	Si–Si	3.17	—		
	Ca–O	2.34	6.5		
15 GPa	O–O	2.60	—	O–Si–O	108.7
	Si–O	1.60	4.1	Si–O–Si	138.3
	Si–Si	3.06	—		
	Ca–O	2.28	7.9		

4. Discussion

4.1. Structural comparison between $CaSiO_3$, $CaMgSi_2O_6$ and $MgSiO_3$ glasses at ambient pressure and temperature

4.1.1. Density and bulk modulus. The densities of the calculated $CaSiO_3$, $CaMgSi_2O_6$ and $MgSiO_3$ glass structures are 2.98, 2.93 and 2.80 g cm^{-3}. These values agree with the experimental densities within 3% (Taniguchi *et al* 1997, Shimoda *et al* 2005).

The MD-derived bulk moduli of $CaSiO_3$, $CaMgSi_2O_6$ and $MgSiO_3$ glasses were calculated to be 53.2, 57.1 and 59.5 GPa by using the third-order Birch–Murnaghan equation (figure 2). The experimental values reported for $CaMgSi_2O_6$ and $MgSiO_3$ glasses are ∼73 and 87.7 GPa, respectively (Kubicki and Lasaga 1991, Askarpour *et al* 1993). This study underestimates the experimental values by 20–30%. However, the present calculations give much improved values contrary to Kubicki and Lasaga (1991) and reproduce the experimental properties reasonably well.

4.1.2. Pairwise distances within SiO_4 tetrahedral species. The Si–O distances in $CaSiO_3$–$MgSiO_3$ MD glass structures were 1.62 Å at 0.1 MPa and 300 K. This is consistent with x-ray

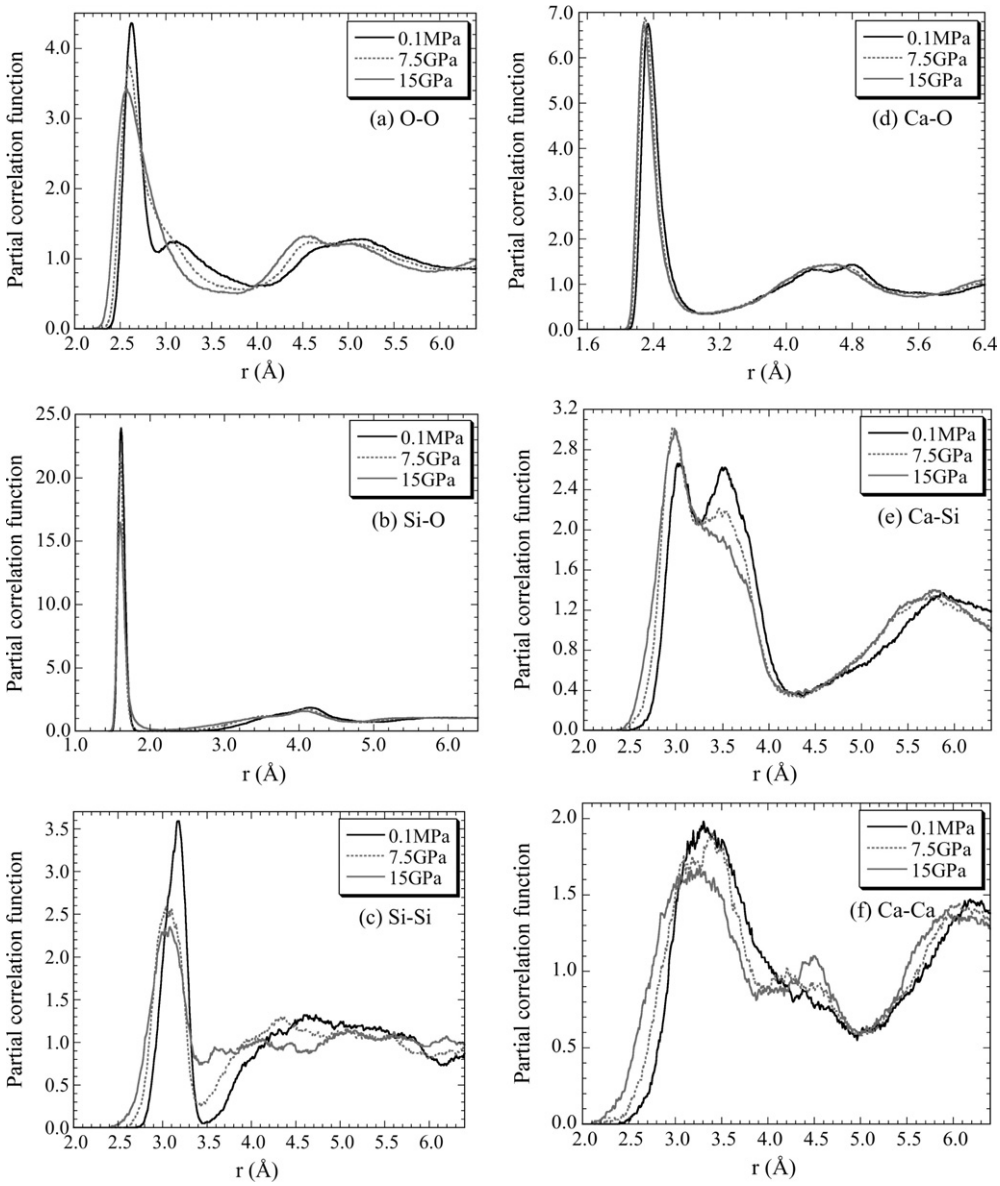

Figure 3. Pair correlation functions of $CaSiO_3$ glass at 0.1 MPa, 7.5 and 15 GPa.

RDF analyses (Yin *et al* 1983, 1986, Taniguchi *et al* 1997). The average Si–O–Si angle of ∼148° was also supported by Shimoda *et al* (2005). These results indicate that the present study successfully reproduces the real glass structures in the short-range scale.

There are no differences in Si–O, O–O pair distances between $CaSiO_3$–$MgSiO_3$ glasses. The O–Si–O angle is obtained to be ∼109.3°, and therefore the regular tetrahedron controls the short-range order. This means that the SiO_4 tetrahedron is not influenced by distinct modifier cations. The present calculation is in contrast to Abramo *et al* (1992), who suggested distortion of the SiO_4 tetrahedron in $CaSiO_3$ glass.

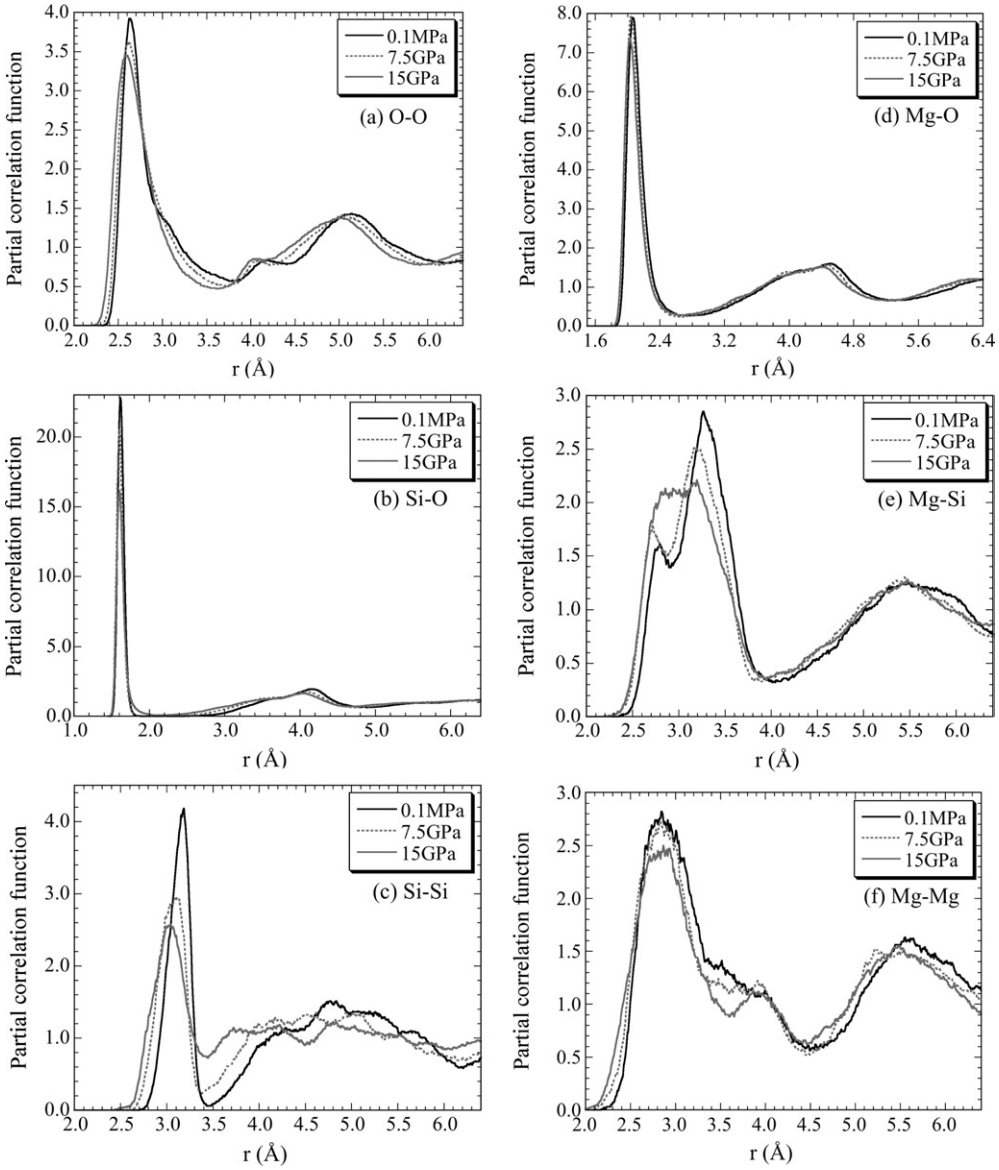

Figure 4. Pair correlation functions of $MgSiO_3$ glass at 0.1 MPa, 7.5 and 15 GPa.

4.1.3. Coordination environments around Ca and Mg ions. The O–O pair correlation function (PCF) for $CaSiO_3$ glass has a small hump at ∼3.10 Å (figure 3(a)). This can be assigned to the O–O distance within a CaO_6 polyhedron (Abramo *et al* 1992). A similar feature is also observed as a shoulder in the O–O PCFs of $CaMgSi_2O_6$ and $MgSiO_3$ glasses.

The average Ca–O distance of $CaSiO_3$ and $CaMgSi_2O_6$ glasses is 2.34 Å, which is slightly shorter than the experimental values (2.37–2.49 Å; Eckersley *et al* 1988, Taniguchi *et al* 1997). We obtained a Ca coordination number of 6.5 for both $CaSiO_3$ and $CaMgSi_2O_6$ glasses. This suggests the predominance of CaO_6 octahedra (Abramo *et al* 1992, Matsui 1996). Experimentally, Gaskell *et al* (1991) have concluded the existence of well-ordered CaO_6 octahedra in the $CaSiO_3$ glass structure by neutron diffraction with Ca isotopic substitution.

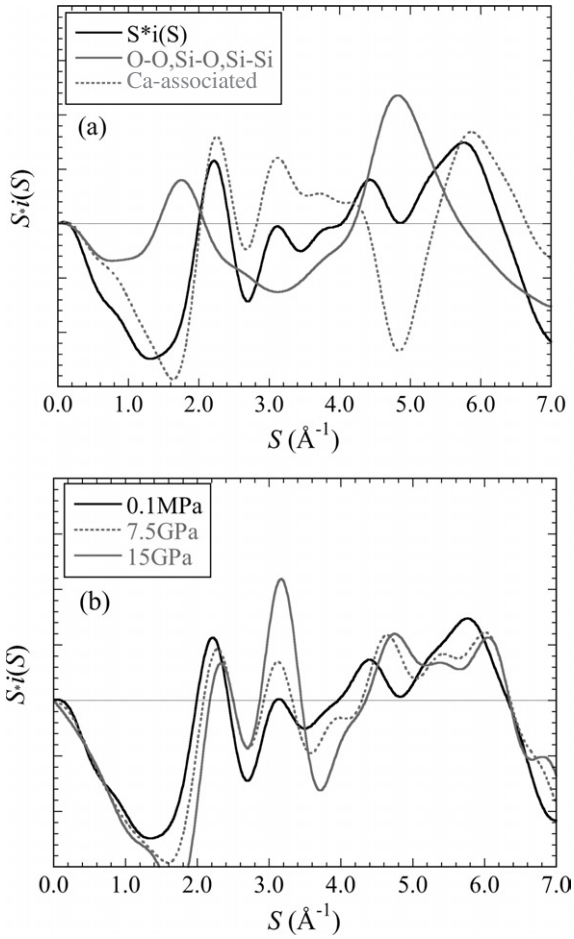

Figure 5. Partial $S{\cdot}i(S)$ curves (a), and total $S{\cdot}i(S)$ curves at 0.1 MPa, 7.5 and 15 GPa (b) for $CaSiO_3$ glass.

Table 3. A list of interatomic distances, bond angles and coordination numbers for $MgSiO_3$ glass at 300 K. The cut-off distances for Si–O and Mg–O coordination are 2.0 and 2.8 Å, respectively.

	Interatomic distance (Å)		Coordination number	Bond angle (deg)	
0.1 MPa	O–O	2.64	—	O–Si–O	109.3
	Si–O	1.62	4.0	Si–O–Si	148.1
	Si–Si	3.17	—		
	Mg–O	2.07	5.7		
15 GPa	O–O	2.57	—	O–Si–O	108.7
	Si–O	1.60	4.1	Si–O–Si	137.6
	Si–Si	3.06	—		
	Mg–O	2.04	6.6		

On the other hand, the Mg coordination environment in $CaMgSi_2O_6$ and $MgSiO_3$ glasses remains controversial. Experimentally, some researchers suggested highly distorted octahedral

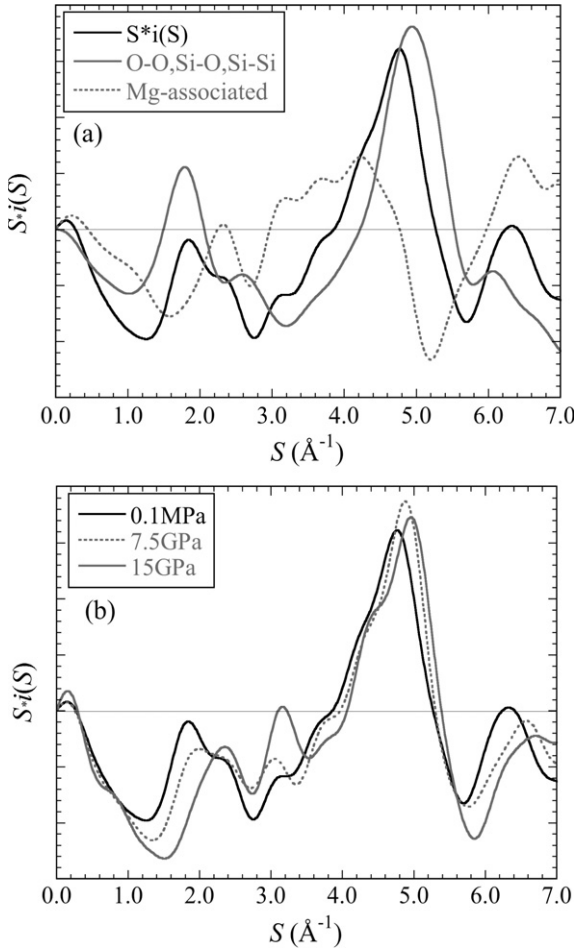

Figure 6. Partial $S{\cdot}i(S)$ curves (a), and total $S{\cdot}i(S)$ curves at 0.1 MPa, 7.5 and 15 GPa (b) for $MgSiO_3$ glass.

Mg species (Yin *et al* 1983, Ildefonse *et al* 1995, Kroeker and Stebbins 2000), whereas others concluded tetrahedral coordination (Hanada *et al* 1988, Taniguchi *et al* 1995, Tabira 1996). Wilding *et al* (2004) have recently reported an average Mg–O distance of 2.2 Å, and an average coordination number of 4.5 by applying a combination of x-ray and neutron diffraction and reverse Monte Carlo simulation to the MgO–SiO_2 system. In the present study, the average Mg–O distance is 2.07 Å, and the Mg coordination is calculated to be 5.7 for $CaMgSi_2O_6$ and $MgSiO_3$ glasses. The previous MD studies concluded tetrahedral coordination with a Mg–O distance of 1.90–1.96 Å (Matsui and Kawamura 1980, Kubicki and Lasaga 1991), while Matsui (1996) provided a coordination number of 5.2 and 1.99 Å, respectively. The inconsistency between the MD results can be attributed to the difference in the applied potential functions and parameters. We here conclude a predominance of the distorted MgO_6 octahedron, in consistency with the x-ray RDF analysis and a reliable NMR result (Yin *et al* 1983, Kroeker and Stebbins 2000).

Figures 3(f) and 4(f) show clear correlations between metal cations (Ca–Ca and Mg–Mg), suggesting their non-random distribution in the glass structures. This is also supported by

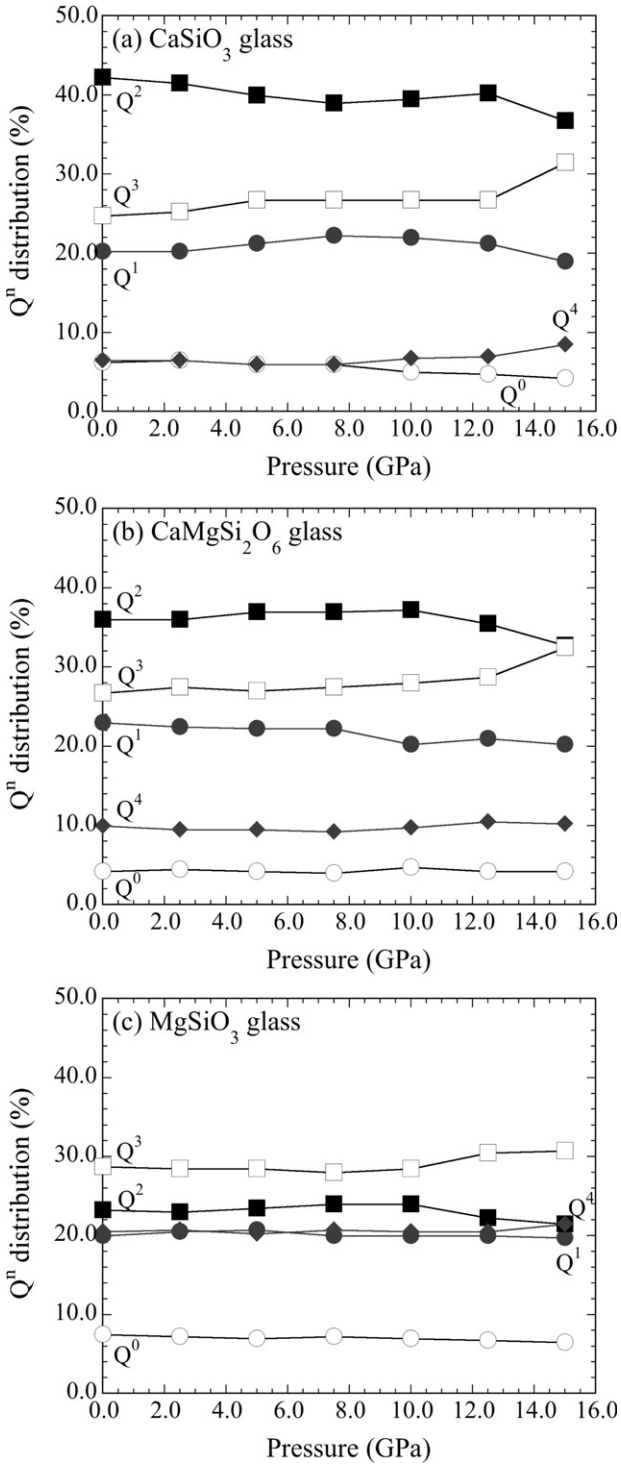

Figure 7. Pressure-induced variations in Q^n distribution of $CaSiO_3$ (a), $CaMgSi_2O_6$ (b) and $MgSiO_3$ (c) glasses.

figures 1(a) and (b) where one can observe Ca- and Mg-rich domains. Gaskell *et al* (1991) postulated *layered* Ca–Ca domains in the $CaSiO_3$ glass structure as in wollastonite, while our MD configurations show up as *clustered* ones.

4.1.4. Calculated x-ray $S{\cdot}i(S)$ curves. The MD-derived $S{\cdot}i(S)$ curves at ambient pressure are in agreement with the published experiments (Taniguchi *et al* 1997). The first sharp diffraction peak (FSDP) positions of MD-derived $S{\cdot}i(S)$ curves were 2.21, 2.10 and 1.86 $Å^{-1}$ for $CaSiO_3$, $CaMgSi_2O_6$ and $MgSiO_3$ glasses, respectively. These are consistent with the experimental values within 5%. On the basis of an analysis of partial $S{\cdot}i(S)$ values, we found that the FSDP of $CaSiO_3$ glass consists of dominant contributions from Ca-associated partial structure factors (figure 5(a)). This is supported by Eckersley *et al* (1988) and Gaskell *et al* (1991), who reported Ca-related neutron-weighted structure factors for $CaSiO_3$ glass and showed a prominent peak at ~ 2 $Å^{-1}$. On the other hand, the FSDP of $MgSiO_3$ glass is composed of SiO_4-associated contributions (figure 6(a)), and the FSDP of $CaMgSi_2O_6$ glass has contributions from both SiO_4 (as in $MgSiO_3$ glass) and Ca component (as in $CaSiO_3$ glass). These results imply the different contributions to FSDP between silicate glasses with distinct chemical compositions.

4.1.5. Q^n distributions in the glass structures. The present study gives the average Q^n species of $n = 2.05$, 2.15 and 2.35 for $CaSiO_3$, $CaMgSi_2O_6$ and $MgSiO_3$ glasses, respectively. The difference in Q^n distributions between $CaSiO_3$ and $MgSiO_3$ glasses is small but significant, and can be related to the polarizing powers or electrostatic field strength of modifier ions (Murdoch *et al* 1985). The present study is consistent with the Raman- and NMR-based Q^n distributions (Frantz and Mysen 1995, Zhang *et al* 1997, Schneider *et al* 2003); for example, Schneider *et al* (2003) reported $n = 2.0$ and 2.1 for $CaSiO_3$ and $CaMgSi_2O_6$ glasses by NMR peak decomposition.

4.2. Pressure-induced structural changes of $CaSiO_3$–$MgSiO_3$ glasses

4.2.1. The atomic distances and coordination numbers. The pair correlation functions (PCFs) for $CaSiO_3$–$MgSiO_3$ glasses showed clear pressure variations (figures 3 and 4 for $CaSiO_3$ and $MgSiO_3$ glasses, respectively). The Si–O first-neighbour peak position did not show significant changes with applied pressure. However, the peak intensity decreases, and a tail emerges at 1.7–1.9 Å. The elongation of some Si–O pairs implies SiO_4 tetrahedral distortion or a minor formation of highly coordinated Si species. The average O–Si–O angle shifted slightly from 109.3° to 108.7° (tables 2 and 3).

The Si–Si distance has clearer changes (figures 3(c) and 4(c)). Under ambient pressure, the Si–Si PCFs show a well-defined first-neighbour peak. There seems to be a large intensity reduction at the first peak between 0.1 MPa and 7.5 GPa, suggesting a significant variation in bond angle distribution even at low pressures. Also, the gap at 3.4–3.8 Å is found to be buried with pressure due to an approach of second neighbours into the first coordination sphere (i.e. a large contraction of the Si–Si(2) distance). The change in first-neighbour Si–Si(1) distance was closely related with Si–O–Si bond angle. The Si–Si(1) distance shifted from 3.17 Å to 3.06 Å ($\Delta = 3.5\%$) and the Si–O–Si bond angle was greatly reduced from 148° to 138° with applied pressure up to 15 GPa (figure 8). The present observation is consistent with Kubicki *et al* (1992), who have reported the bond angle reduction in $CaSiO_3$–$MgSiO_3$ glasses under pressure by *in situ* high pressure Raman spectroscopy.

Figure 8 appears to show a quasi-linear dependence of Si–O–Si angle variation as a function of pressure up to 15 GPa. We obtained a coefficient of about $-0.7°$ GPa^{-1} (cf $-1.9°$ GPa^{-1} for SiO_2 glass). This is suggestive of the structural incompressibility (i.e. larger

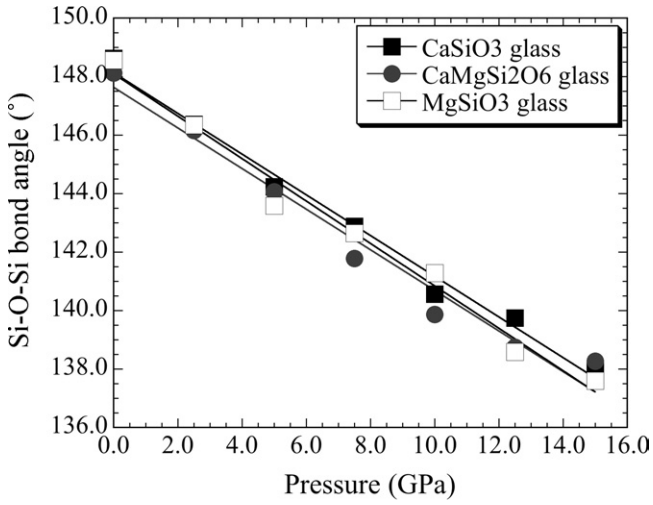

Figure 8. Pressure dependence of average Si–O–Si bond angle. The straight lines are guides to the eyes.

bulk modulus) of $CaSiO_3$–$MgSiO_3$ glasses relative to SiO_2 glass, owing to the existence of modifier cations in $CaSiO_3$–$MgSiO_3$ glasses. The interstitial cations prevent the large compaction that occurs in SiO_2 glass. We note that no significant differences are recognized in the pressure variations of the bond angle between $CaSiO_3$–$MgSiO_3$ glasses.

The Ca–O distance showed a relatively large contraction by ∼2.6%, although Mg–O showed a smaller one. This supports Kubicki *et al* (1992), who suggested Ca–O contraction under pressure. The present study presents an increase of Ca and Mg coordination from 6.5 to 7.9, and 5.7 to 6.6, respectively.

On the other hand, the Si coordination change was negligible in $CaSiO_3$–$MgSiO_3$ glasses. This is consistent with previous works, reporting the onset of coordination change above 15–20 GPa (Hemley *et al* 1986, Meade *et al* 1992, Williams *et al* 1993, Wolf and McMillan 1995). The coordination increase involves an increase of the average Si–O distance (Kubicki and Lasaga 1991). Instead, our simulation shows a slight decrease up to 15 GPa.

Moreover, Ca–Si and Mg–Si PCFs show pressure variations of the first coordination peak at 2.5–4.0 Å (figures 3(e) and 4(e)). Doublet peaks are observed at 3.0 and 3.5 Å in Ca–Si pairs, and at 2.8 and 3.3 Å in Mg–Si pairs, corresponding to edge- and corner-shared distances, respectively, between a Ca- or Mg-coordination polyhedron and a SiO_4 tetrahedron. One can observe an increase in edge-sharing relative to corner-linkage with increasing pressure.

4.2.2. Structural evolutions in medium-range scale. We obtained the pressure-induced modifications in $S{\cdot}i(S)$ curves in the low-S region (figures 5(b) and 6(b) for $CaSiO_3$ and $MgSiO_3$ glasses). A position shift and an intensity decrease of the FSDP feature were observed with a linear relation as a function of pressure. An intensity increase of the second peak at ∼3.0 $Å^{-1}$ was also observed. Similar changes were reported for SiO_2 glass from an MD simulation (Jin *et al* 1993, 1994) and x-ray diffraction studies (Meade *et al* 1992, Inamura *et al* 2001). The FSDP position (S_1) can be associated to the averaged 'cell' dimension, d_m ($=2\pi/S_1$), of medium-range structural units (Tan and Arndt 1999). In the case of depolymerized glasses, the positive shift of the FSDP position can be considered as a compaction of the clusters dominated by SiO_4 anionic species (Q^n) and Ca, Mg coordination

polyhedra (Shimoda *et al* 2005). This is supposed to involve a significant contraction of the Si–Si(2) distance, as mentioned above.

Kubicki and Lasaga (1991) discussed the pressure-induced changes in the Q^n distribution for a $MgSiO_3$ melt at 5000 K. They reported decreases of Q^0, Q^1 and Q^2 species and a relative increase of Q^3 species with increasing pressure. In the present study, a similar result is obtained: a decrease of Q^2 species and an increase of Q^3 species (figure 7). The average Q^n species increase moderately to $n = 2.21$, 2.24 and 2.41 at 15 GPa for $CaSiO_3$, $CaMgSi_2O_6$ and $MgSiO_3$ glasses, respectively. Xue *et al* (1989) and Dickinson *et al* (1990) have reported pressure-induced disproportionation reactions, $2Q^n = Q^{n-1} + Q^{n+1}$ ($n = 1$–3), for alkali silicate melts, based on NMR and Raman spectroscopy. The changes in Q^n distribution under pressure can be associated to ionic diffusivity or bulk viscosity (Kubicki and Lasaga 1991, Dickinson *et al* 1990, Xue *et al* 1989, 1991; also see a review by Wolf and McMillan (1995)). Scarfe *et al* (1979) showed an increase in viscosity with pressure for $CaMgSi_2O_6$ melt. Angell *et al* (1987) and Shimizu and Kushiro (1991) reported a decrease in ionic diffusivity at moderate pressure for $CaMgSi_2O_6$ melt. Pressure-induced evolutions in the diffusivity and viscosity of such depolymerized melts can be explained in terms of melt polymerization; the polymerization of Q^0, Q^1 or Q^2 species to Q^3 or Q^4 prohibits the diffusions of Si^{4+} and O^{2-} ions and increases the size of flow units, resulting in the increase of bulk viscosity. Dickinson *et al* (1990) speculated that the polymerization could be a primary compression mechanism of depolymerized silicate melts at low pressures. The polymerization further predicts excess *free* oxygens bonded to only Ca^{2+}, Mg^{2+} ions. These oxygens can be associated to the significant formation of highly coordinated Ca and Mg species ($>\sim 6$) at pressures up to 15 GPa.

5. Conclusion

The pressure-induced structural evolutions of $CaSiO_3$–$MgSiO_3$ glasses have been examined in detail by means of molecular dynamics simulation. The empirical potential parameters used in this study were shown to be applicable to amorphous phases as well as crystalline materials. We obtained a Mg coordination number of 5.7 under ambient pressure, which is consistent with a reliable ^{25}Mg NMR result (Kroeker and Stebbins 2000).

A detailed examination of partial $S{\cdot}i(S)$ curves indicated that the structural components, which have dominant contributions to the FSDP feature, could be different even between $CaSiO_3$ and $MgSiO_3$ glasses.

In the present study, the main compression mechanisms for $CaSiO_3$–$MgSiO_3$ metasilicate glasses are concluded to be: (1) the Si–O–Si angle reduction, (2) the coordination increase of Ca and Mg modifier cations, and (3) the compaction at the medium-range scale. We did not find significant differences in the pressure responses between $CaSiO_3$–$MgSiO_3$ glasses. This may imply that the structural changes of SiO_4 framework units are more important than those of interstitial cations, Ca and Mg.

Acknowledgments

We thank Professor Kawamura for providing MXDORTO codes, and Dr Shiraki for his valuable suggestions.

References

Abramo M C, Caccamo C and Pizzimenti G 1992 *J. Chem. Phys.* **96** 9083–91
Angell C A, Cheeseman P A and Kadiyala R 1987 *Chem. Geol.* **62** 85–95

Askarpour V, Manghnani M H and Richet P 1993 *J. Geophys. Res.* **98** 17683–9
Clark J R, Appleman D E and Papike J J 1969 *Mineral. Soc. Am. Special Paper* **2** 31–50
Dickinson J E, Scarfe C M and McMillan P 1990 *J. Geophys. Res.* **95** 15675–81
Eckersley M C, Gaskell P H, Barnes A C and Chieux P 1988 *Nature* **335** 525–7
Ekunwe N S and Lacks D J 2002 *Phys. Rev.* B **66** 212101–4
Frantz J D and Mysen B O 1995 *Chem. Geol.* **121** 155–76
Gaskell P H, Eckersley M C, Barnes A C and Chieux P 1991 *Nature* **350** 675–7
Hanada T, Soga N and Tachibana T 1988 *J. Non-Cryst. Solids* **105** 39–44
Hemley R J, Mao H K, Bell P M and Mysen B O 1986 *Phys. Rev. Lett.* **57** 747–50
Ildefonse P, Calas G, Flank A M and Lagarde P 1995 *Nucl. Instrum. Methods Phys. Res.* B **97** 172–5
Inamura Y, Arai M, Nakamura M, Otomo T, Kitamura N, Bennington S M, Hannon A C and Buchenau U 2001 *J. Non-Cryst. Solids* **293–295** 389–93
Jin W, Kalia R K, Vashista P and Rino J P 1993 *Phys. Rev. Lett.* **71** 3146–9
Jin W, Kalia R K, Vashista P and Rino J P 1994 *Phys. Rev.* B **50** 118–31
Kawamura K 1996 MXDORTO. Japan Chemistry Program Exchange, P029
Kroeker S and Stebbins J F 2000 *Am. Mineral.* **85** 1459–64
Kubicki J D, Hemley R J and Hofmeister A M 1992 *Am. Mineral.* **77** 258–69
Kubicki J D and Lasaga A C 1991 *Phys. Chem. Minerals* **17** 661–73
Matsui M 1996 *Geophys. Res. Lett.* **23** 395–8
Matsui Y and Kawamura K 1980 *Nature* **285** 648–9
Meade C, Hemley R J and Mao H K 1992 *Phys. Rev. Lett.* **69** 1387–90
Miyake A 1998 *Mineral. J.* **20** 189–94
Morimoto N 1960 *Z. Kristallogr.* **114** 120–47
Murdoch J B, Stebbins J F and Carmichael I S E 1985 *Am. Mineral.* **70** 332–43
Ohashi Y 1984 *Phys. Chem. Minerals* **10** 217–29
Peacor D R and Prewitt C T 1963 *Am. Mineral.* **48** 588–96
Pilla O, Angelani L, Fontana A, Conçalves J R and Ruocco G 2003 *J. Phys.: Condens. Matter* **15** S995–1005
Scarfe C M, Mysen B O and Virgo D 1979 *Carnegie Inst. Washington Yearb.* vol 78 , pp 547–51
Schneider J, Mastelaro V R, Zanotto E D, Shakhmatkin B A, Vedishcheva N M, Wright A C and Panepucci H 2003 *J. Non-Cryst. Solids* **325** 164–78
Shimizu N and Kushiro I 1991 *Adv. Phys. Geochem.* **9** 192–212
Shimobayashi N, Miyake A, Kitamura M and Miura E 2001 *Phys. Chem. Minerals* **28** 591–9
Shimoda K, Miyamoto M, Kikuchi M, Kusaba K and Okuno M 2005 *Chem. Geol.* **222** 83–93
Tabira Y 1996 *Mater. Sci. Eng.* B **41** 63–6
Tan C Z and Arndt J 1999 *J. Non-Cryst. Solids* **249** 47–50
Taniguchi T, Okuno M and Matsumoto T 1995 *Mineral. J.* **17** 231–44
Taniguchi T, Okuno M and Matsumoto T 1997 *J. Non-Cryst. Solids* **211** 56–63
Trachenko K and Dove M T 2003 *Phys. Rev.* B **67** 064107–17
Tse J S, Klug D D and Page Y L 1992 *Phys. Rev.* B **46** 5933–8
Tsuneyuki S and Matsui Y 1995 *Phys. Rev. Lett.* **74** 3197–200
Valle R G D and Venuti E 1996 *Phys. Rev.* B **54** 3809–16
Wilding M C, Benmore C J, Tangeman J A and Sampath S 2004 *Chem. Geol.* **213** 281–91
Williams Q, Hemley J, Kruger M B and Jeanloz R 1993 *J. Geophys. Res* **98** 22157–70
Wolf G H and McMillan P F 1995 Pressure effects on silicate melt: Structure and properties *Structure, Dynamics and Properties of Silicate Melts* (*Reviews in Mineralogy* vol 32) ed J F Stebbins *et al* (Washington, DC: MSA) pp 505–61
Xue X, Stebbins J F, Kanzaki M, Poe B and McMillan P 1991 *Am. Mineral.* **76** 8–26
Xue X, Stebbins J F, Kanzaki M and Tronnes R G 1989 *Science* **245** 962–4
Yin C D, Okuno M, Morikawa H and Marumo F 1983 *J. Non-Cryst. Solids* **55** 131–41
Yin C D, Okuno M, Morikawa H, Marumo F and Yamanaka T 1986 *J. Non-Cryst. Solids* **80** 167–74
Zhang P, Grandinetti P J and Stebbins J F 1997 *J. Phys. Chem.* B **101** 4004–8